RSC Advances

PAPER

View Article Online
View Journal | View Issue



Cite this: *RSC Adv.*, 2026, **16**, 12702

# Benzo[*d*]imidazole anchored oxadiazole derivatives: synthesis, characterization, biological evaluation, *in silico* docking and ADME-T analysis

Yellamanda Rao Salluri, [a] Kalyani Chepuri [b] and Shaik Anwar *[a]

A novel series of 1,2,4-oxadiazoles based on benzo[*d*]imidazole-1,3,4-oxadiazole fused 1,2,4-oxadiazoles, were synthesised. The proposed chemical structures of the novel hybrids were confirmed by a variety of spectroscopic methods, including HRMS, NMR ($^{1}H/^{13}C$), and infrared. The antibacterial properties of these compounds showed that compound **8b** (37 ± 1.20 mm) and compound **8i** (6.9 ± 1.01 μM) had the highest zone of inhibition (ZI) and lowest minimum inhibitory (MIC) values against *S. aureus* ATCC 29213, which was verified by *in silico* evaluation. Compound **8f** exhibited considerably better antibacterial activity (31 ± 0.19 mm) against *S. epidermidis* ATCC 12228, and scaffold **8f** showed a significantly higher antibacterial effect (31 ± 0.19 mm) against *S. pyogenes* ATCC 19615 compared to moxifloxacin (29 ± 0.16 mm). Finally, *in silico* research that includes molecular modelling also validates an *in vitro* investigation and explains the strong binding pattern of **8b**, **8f**, **8i**, and **8k** against *E. coli* Topoisomerase IV (PDB: 3FV5) and *S. aureus* GyrB (PDB: 4URN). Extending our exploration, an analysis of the ADME-Tox profiling confirmed the safe use of these newly synthesized scaffolds, paving the way for promising therapeutic applications in the field of antimicrobial therapy.

Received 30th November 2025
Accepted 20th February 2026

DOI: 10.1039/d5ra09260d

rsc.li/rsc-advances



## 1 Introduction

As a rising concern to world health, antibiotic resistance increases morbidity, mortality, and medical expenses.[1] Since many bacterial isolates are becoming more resistant to numerous drugs, bacterial illnesses are seen as a global issue. Every year, almost 700 000 people die from diseases that cannot be cured.[2] Experts estimate that more than 10 million people would die from various antibiotic resistances globally by 2050 if the problem is not resolved. Severe infections, which greatly worsen suffering in people with compromised immune systems and result in major morbidity and mortality, are commonly caused by a variety of pathogenic microorganisms, including bacteria, fungi, yeasts, and viruses.[3] Antimicrobial resistance (AMR), which has been exacerbated by the COVID-19 pandemic, has posed a serious danger to public health and global economic development.[4] While there are several reasons for this, the increase in HIV-positive patients and the number of cancer patients undergoing chemotherapy are two important ones.[5] Thankfully, other antibiotics have been approved for commercial use through structural modification of tetracyclines, quinolones and aminoglycosides, and other compounds, such as plazomicin, delafloxacin, moxifloxacin, and gemifloxacin. At the same time, certain natural antibacterial compounds have been the subject of clinical studies.[6] As a result, researchers are now looking for novel molecular targets for antimicrobial drugs. Therefore, there is a continuing need for new antimicrobial drugs that can specifically target various bacteria without interfering with the metabolic functions of the host.

Numerous researchers in medicinal chemistry have been drawn to the promising findings in the chemistry, structure–activity relationship, and biological activities of various heterocycles, particularly interested in the synthesis of benzimidazole and its derivatives. Heterocyclic compounds, especially nitrogen heterocycles, make up a substantial class of chemicals utilized in the pharmaceutical business and account for almost 60% of all pharmacological medications.[7] Benzimidazole scaffold exhibit high aromaticity and metabolic stability, which is advantageous for drug availability and efficacy. Its heteroatoms facilitate key interactions, such as hydrogen bonding and hydrophobic interactions, with various biological targets, including enzymes (*e.g.*, β-tubulin, ChE inhibitors) and α-amylase and α-glucosidase inhibitors. The thiadiazole moiety can also inhibit DNA/RNA synthesis, contributing to its broad-spectrum of activity observed in several FDA-approved drugs like albendazole, tiabendazole, benomyl, enviradene, and bendamustine have been used as

[a]*Department of Chemistry, School of Applied Science and Humanities, Vignan's Foundation for Science, Technology and Research, Vadlamudi, Guntur 522 213, Andhra Pradesh, India. E-mail: shaikanwarcu@gmail.com; drsa_sh@vignan.ac.in; Tel: (+91)-8632344777*

[b]*Centre for Biotechnology, University College of Engineering Science and Technology Hyderabad, Jawaharlal Nehru Technological University Hyderabad, Hyderabad 500085, India*

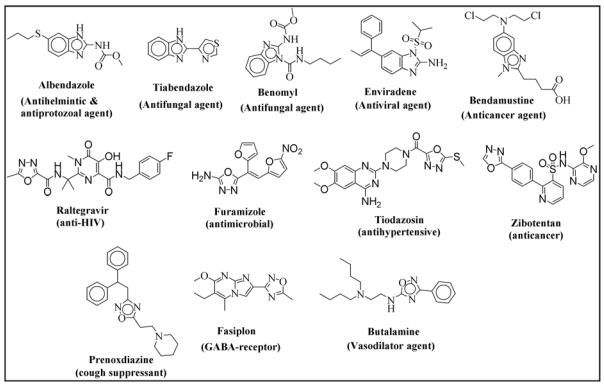


Fig. 1 Commercial medications chemical structures based on 1,3,4-oxadiazole, 1,2,4-oxadiazoles, and benzo[*d*]imidazole.

fungicidal agents in the market (Fig. 1). An extensive pharmacological framework of benzimidazole has been reported in a number of publications. These include antibacterial,[8] antifungal,[9] antituberculosis,[10] antiviral,[11] antimalarial,[12] antiulcer,[13] antileishmanial,[14] anti-inflammatory,[15] antidiabetic,[16] antiprotozoal,[17] anti-convulsant,[18] antioxidant,[19] anti-hypertensive,[20] anti-Alzheimer, and analgesic.[21]

The analogues of 1,3,4-oxadiazole and imidazole are the basic building blocks of many medications.[22] This class of heterocycles contains compounds that have demonstrated a wide range of therapeutic potential, including antibacterial,[23] antiepileptic,[24] anticancer,[25] antiviral,[26] and anti-inflammatory properties.[27] Commercial medications such as Raltegravir (anti-HIV), Furamizole (antimicrobial), Zibotentan (anticancer), Tiodazosin (antihypertensive), Nesapidil (vasodilator), and Fenadiazole (sedative) all contain the 1,3,4-oxadiazole molecule, which has proven pharmacophore status (Fig. 1).[28] The hydrophilic and electron-donating characteristics oxadiazole ring allows for non-covalent binding with enzyme and other biomolecules, nitrogenated-based heterocycles, like 1,2,4-oxadiazole-derived molecules, exhibit encouraging biological activity.[29] Numerous bioactive qualities, such as antibacterial,[30] anticancer,[31] antitubercular,[32] anti-inflammatory, and antiparasitic activities,[33] have since been shown by studies on 1,2,4-oxadiazole derivatives. Additionally, a 1,2,4-oxadiazole moiety is present in the molecular structure of clinically used medications like Oxolamine, Prenoxdiazine, Irrigor, Fasiplon (GABA-receptor), and Butalamine (vasodilatation agent), respectively. This emphasizes how crucial this moiety is to drug discovery and design (Fig. 1).[34]

Recent studies highlight that 1,3,4-oxadiazole derivatives are increasingly important as privileged scaffolds in medicinal chemistry, with advancements focused on overcoming drug resistance and improving the efficiency of synthesis. The novelty in recent literature lies in the shift toward conventional/microwave synthetic methodologies that produce high yields, as well as the design of hybrid molecules that target complex, multidrug-resistant infections and cancer cell lines. Molecular hybridization is a powerful strategy in medicinal chemistry and drug discovery where two or more pharmacophoric units from different bioactive substances are combined into a single molecule. This approach aims to create a new hybrid compound with enhanced affinity, improved efficacy, altered selectivity profiles, and/or dual modes of action, often resulting in superior properties compared to the parent compounds or simple combination therapies. In this work, a series of benzo[*d*]imidazole derivatives with 1,2,4-oxadiazole and 1,3,4-oxadiazole groups are synthesized and evaluated, *in silico* modeling and biological evaluation.[35] We anticipate that this study will increase our understanding of how the pharmacological action of oxadiazole derivatives of benzimidazole is influenced by their chemical structure. The aromatic rings benzimidazole and *bis*-oxadiazole both add to the molecule's overall rigidity and planarity, which is advantageous for attaching to biological targets. The structural flexibility and varied substituent patterns on both rings increase the potential for fine-tuning the compounds for specific therapeutic outcomes. The findings of this study may contribute for novel antimicrobial drugs with enhanced selectivity and efficacy, expanding the range of chemotherapeutic alternatives for the treatment of bacteria. The present heterocyclic work offers significant practical and conceptual advantages by addressing the need for more efficient, sustainable, and functionalized chemical synthesis in the pharmaceutical and materials science industries.

## 2 Results and discussion

This study used the Vilsmeier reaction sequence shown in Scheme 1 to synthesize a new series of 1,2,4-oxadiazole based on benzo[*d*]imidazole-1,3,4-oxadiazole. We have prepared compounds number **1–3** based on previous literature.[36] Methyl 3-(1,5-dimethyl-1*H*-benzo[*d*]imidazole-2-yl)propanoate (**1**) and hydrazine hydrate were refluxed for approximately 10 hours at 75 °C with methanol present. 5-[2-(1,5-Dimethyl-1*H*-1,3-benzodiazol-2-yl)ethyl]-1,3,4-oxadiazole-2-thiol (**3**) was obtained by refluxing the reaction mixture for eight hours after the hydrazide (**2**) further reacted with carbon disulphide and potassium hydroxide in ethanol. The yield was excellent, at 90%. Additionally, in the presence of potassium carbonate at room temperature, the oxadiazole (**3**) was transformed into propargylation in the presence of 2-bromoacetonitrile as a light-brown solid (**4**). The key intermediate (**5**) was synthesized by the reaction of (**4**) in DCM in the presence of mCPBA at 0 °C for 2 h. (*Z*)-2-{[5-[2-(1,5-Dimethyl-1*H*-benzimidazol-2-yl)ethyl]-1,3,4-

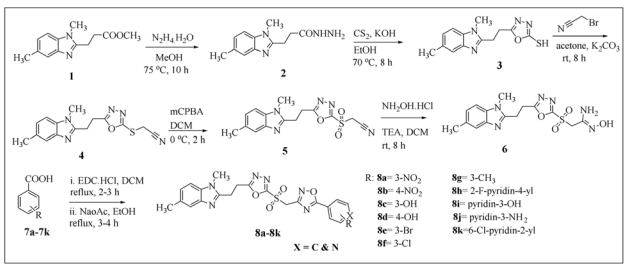


Scheme 1 Synthesis of benzo[*d*]imidazole-substituted oxadiazole derivatives (**8a–8k**).

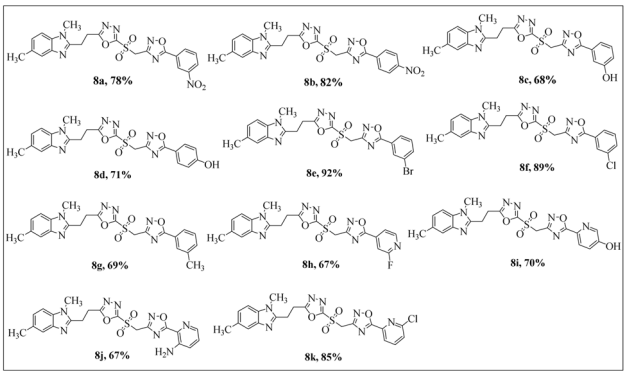


Fig. 2 Synthesized oxadiazole scaffolds.

oxadiazol-2-yl]sulfonyl}-*N*′-hydroxyethanimidamide (**6**) was create when a combination of TEA and hydroxylamine hydrochloride was added dropwise to DCM at rt. *O*-Acylation and cyclization steps were conducted in a one-pot reaction with the carboxylic acids in the presence of coupling reagent 1-ethyl-3-(3-dimethylaminopropyl) carbodiimide hydrochloride (EDC.HCl). Next, 1,2,4-oxadiazoles were obtained through reflux of the acylated intermediate in ethanol in the presence of sodium acetate (Scheme 1).[37] The 1,2,4-oxadiazole derivatives were then formed as a result of component (**6**) and the corresponding acids (**7a–7k**) in refluxing DCM for eight hours in the presence of EDC.HCl. Ultimately, the obtained intermediate was refluxed in the presence of sodium acetate in ethanol for 3–4 hours. Reaction progress was monitored by TLC (2 : 8; ethyl acetate and hexane). After completion, the reaction solvent was distilled out, then 2 N NaOH was added, followed by extraction with ethyl acetate. The separated organic layer was distilled, and the crude was purified by flash column chromatography to produce compounds (**8a–8k**) (67–92%) (Fig. 2).

### 2.1 Antibacterial activity

Three Gram-negative strains, *Escherichia coli* ATCC 25922, *Klebsiella pneumonia* ATCC 13883, and *Pseudomonas aeruginosa* ATCC 27853, as well as three Gram-positive strains, *Streptococcus pyogenes* ATCC 19615, *Staphylococcus epidermidis* ATCC 12228, and *Staphylococcus aureus* ATCC 29213, were used to test the titled derivatives (**8a–8k**) *in vitro* antibacterial activity. Title substances antibacterial inhibitory activity was tested using a previously established agar wall diffusion technique. The diameter zone of inhibition (ZI) and minimal inhibitory concentration (MIC) values for the investigated derivatives are displayed in Tables 1 and 2.[38] The results indicated that the derivatives antibacterial activity was greatly impacted by the sort and makeup of the substituents on the oxadiazole moiety and phenyl ring. The tested compounds (**8a–8k**) showed moderate to good antibacterial effectiveness against Gram-negative bacteria as compared to Gram-positive bacteria. When compared to the conventional moxifloxacin and gemifloxacin, all compounds showed moderate antibacterial activity. Oxadiazole compound **8b**, which had a zone of inhibition of 37 ± 1.20 mm and significant antibacterial activity against *S. aureus* ATCC 29213, was used as a positive control based on the findings of antibacterial screening. The results revealed that the highest *S. pyogenes* ATCC 19615 inhibition potential is exhibited by compound **8f** with ZI value of 31 ± 0.19 mm. Additionally, compounds **8b** ($IC_{50}$ 32 ± 0.30 mm) and **8i** (ZI = 30 ± 0.38 mm) also showed potent activity against the *S. epidermidis* ATCC 12228 strain. The other derivatives have significant inhibitory antibacterial activity on *S. epidermidis* ATCC 12228 within the ZI values (8 ± 0.87–24 ± 1.08 mm), whereas compounds **8a**, **8f** and **8k** did not show antibacterial inhibition activity against *S. epidermidis*.

Notably, 3-chlorophenyl (**8f**), pyridin-3-ol (**8i**), and 6-chloropyridin-2-yl (**8k**) linked to benzo[*d*]imidazole showed the

Table 1 Antibacterial activity of benzo[*d*]imidazolyl-oxadiazole derivatives (8a–8k)[a]

| Mean diameter of zones of inhibition (mean ± SEM) (mm) | | | | | | |
|---|---|---|---|---|---|---|
| | Gram-positive strains | | | Gram-negative strains | | |
| Entry | *S. pyogenes* ATCC 19615 | *S. epidermidis* ATCC 12228 | *S. aureus* ATCC 29213 | *K. pneumonia* ATCC 13883 | *E. coli* ATCC 25922 | *P. aeruginosa* ATCC 27853 |
| **8a** | 14 ± 0.14 | NA | 20 ± 0.33 | 13 ± 0.20 | NA | 31 ± 0.78 |
| **8b** | 28 ± 0.10 | 32 ± 0.30 | 37 ± 1.20 | NA | 34 ± 1.12 | 13 ± 1.17 |
| **8c** | 10 ± 0.55 | 19 ± 1.03 | NA | 22 ± 0.11 | 25 ± 0.05 | NA |
| **8d** | NA | 8 ± 0.87 | 17 ± 0.04 | 19 ± 0.24 | 11 ± 0.09 | 9 ± 0.62 |
| **8e** | 27 ± 0.99 | 22 ± 0.55 | 16 ± 0.80 | 11 ± 0.08 | NA | NA |
| **8f** | 31 ± 0.19 | NA | 30 ± 0.37 | 29 ± 0.83 | 28 ± 0.10 | 12 ± 0.89 |
| **8g** | NA | 12 ± 0.73 | 15 ± 0.57 | 17 ± 0.28 | NA | 17 ± 1.10 |
| **8h** | 11 ± 0.43 | 9 ± 0.79 | NA | 20 ± 0.05 | 10 ± 0.83 | 23 ± 0.90 |
| **8i** | 28 ± 0.22 | 30 ± 0.38 | 26 ± 0.92 | 28 ± 0.73 | 36 ± 0.13 | NA |
| **8j** | NA | 24 ± 1.08 | 21 ± 1.04 | NA | 14 ± 1.35 | 30 ± 0.75 |
| **8k** | 26 ± 0.32 | NA | 32 ± 0.80 | NA | 25 ± 0.51 | 28 ± 1.10 |
| MXF | 29 ± 0.16 | 31 ± 0.08 | 34 ± 0.62 | 30 ± 0.28 | 33 ± 0.23 | 26 ± 0.79 |
| GMF | 30 ± 0.94 | 28 ± 0.37 | 31 ± 0.16 | 29 ± 0.28 | 35 ± 0.77 | 29 ± 0.40 |

[a] MXF: moxifloxacin; GMF: gemifloxacin; NA: not active; each value is an average of three replicates, ± denotes standard deviation among triplicates.

Table 2 MIC values of the most active analogues against various microbial species (μM)

| Mean diameter of zones of inhibition (mean ± SEM) (mm) | | | | | | |
|---|---|---|---|---|---|---|
| | Gram-positive strains | | | Gram-negative strains | | |
| Entry | *S. pyogenes* ATCC 19615 | *S. epidermidis* ATCC 12228 | *S. aureus* ATCC 29213 | *K. pneumonia* ATCC 13883 | *E. coli* ATCC 25922 | *P. aeruginosa* ATCC 27853 |
| **8b** | 14.7 ± 1.20 | 9.2 ± 0.09 | >50 | 27.4 ± 0.70 | 30.3 ± 1.20 | >50 |
| **8f** | 42.8 ± 0.91 | >50 | 40.2 ± 1.23 | 8.0 ± 1.03 | >50 | 10.5 ± 1.22 |
| **8i** | >50 | 18.9 ± 1.15 | 6.9 ± 1.01 | 19.3 ± 1.65 | 7.0 ± 1.35 | >50 |
| **8k** | 7.3 ± 0.85 | >50 | 37.1 ± 0.67 | >50 | 20.6 ± 1.60 | 22.9 ± 0.55 |
| MXF | 8.2 ± 1.10 | 10.4 ± 0.80 | 7.3 ± 0.92 | 9.1 ± 1.18 | 8.9 ± 1.07 | 12.8 ± 1.02 |
| GMF | 10.4 ± 0.14 | 10.0 ± 1.06 | 8.5 ± 1.12 | 10.5 ± 1.01 | 8.5 ± 0.87 | 11.3 ± 0.54 |

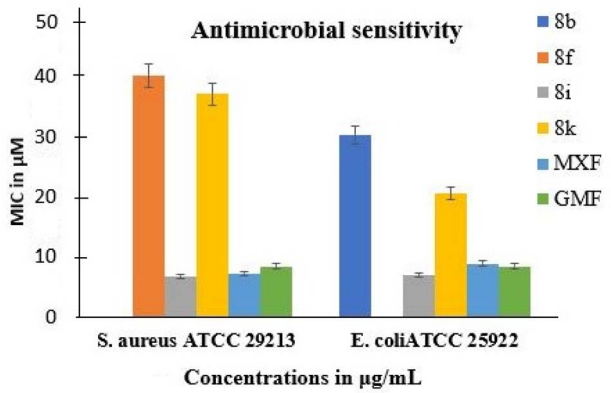


Fig. 3 Antibacterial efficacy of the tested benzo[*d*]imidazoles on the *S. aureus* and *E. coli*.

highest inhibitory effect against *S. aureus* ATCC 29213, with ZI values of 30 ± 0.37, 26 ± 0.92, and 32 ± 0.80 mm (GMF at 31 ± 0.16 mm). Against *K. pneumoniae* ATCC 13883, however, compound 4-hydroxyphenyl-1,2,4-oxadiazole (**8d**), 3-tolyl-1,2,4-oxadiazole (**8g**), and 3-fluoropyridin-4-yl-1,2,4-oxadiazole (**8h**) showed moderate activity (ZI = 19 ± 0.24, 17 ± 0.28, and 20 ± 0.05 mm). In comparison to MXF (ZI = 33 ± 0.23 mm), compound **8b**, which has a 4-nitro group at the 4th position with phenyl, and compound **8i**, which has a hydroxy group at the 3rd position with pyridine, are the lead compounds of the series. They have the highest inhibitory action against *E. coli* ATCC 25922 (ZI values of 34 ± 1.12 and 36 ± 0.13 mm). Then, in 1,2,4-oxadiazole analogues **8a**, **8h**, and **8j**, we found 3-nitrophenyl, 3-fluoropyridin-4-yl, and pyridin-2-amine with ZI values of 31 ± 0.78, 23 ± 0.90, and 30 ± 0.75 mm against *P. aeruginosa* ATCC 27853. These compounds demonstrated superior potency in comparison to MXF (ZI = 26 ± 0.79 mm). The ATCC 27853 strain of *P. aeruginosa* was not susceptible to the antibacterial activity of compounds **8c**, **8e**, and **8i**. Compared to counterparts with electron-withdrawing substituents like $NO_2$ and F, those with electron-donating substituents (such as Br, $NH_2$, and $CH_3$) show less antibacterial activity. Compared to a nitro group at the third position in **8a**, the presence of a nitro group at the fourth position on the phenyl ring in **8b** demonstrated the strongest antibacterial activity. The antibacterial activity of substituted halogen compounds increased when the chlorine atom (**8f**) replaced the bromine atom (**8e**). The results showed

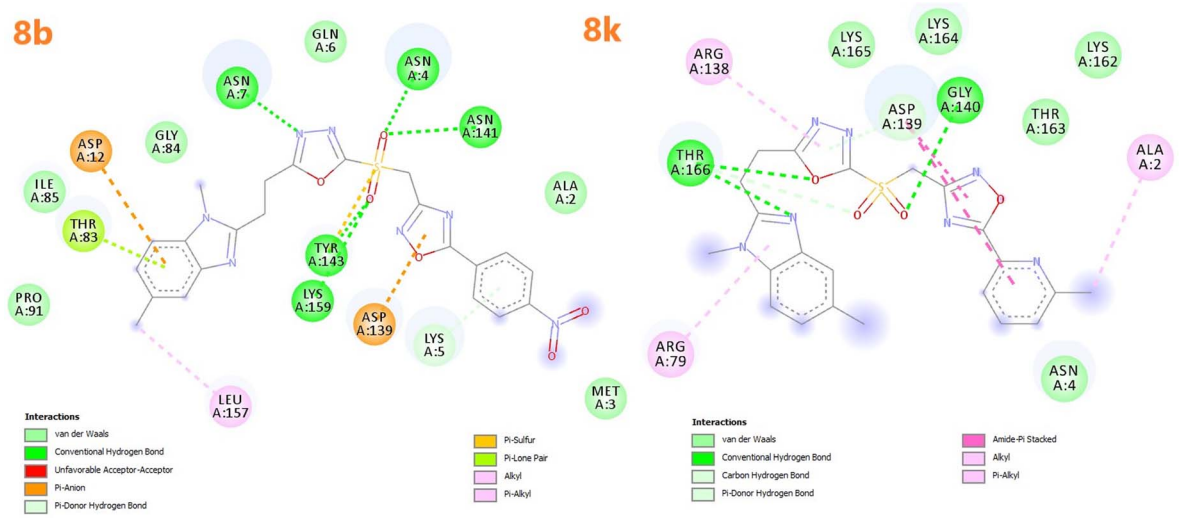


Fig. 4 The active sites of *S. aureus* GyrB [PDB code: 4URN] are bound by ligands **8b** and **8k**, respectively, demonstrating ionic interactions, hydrophobic contacts, and hydrogen bonds.

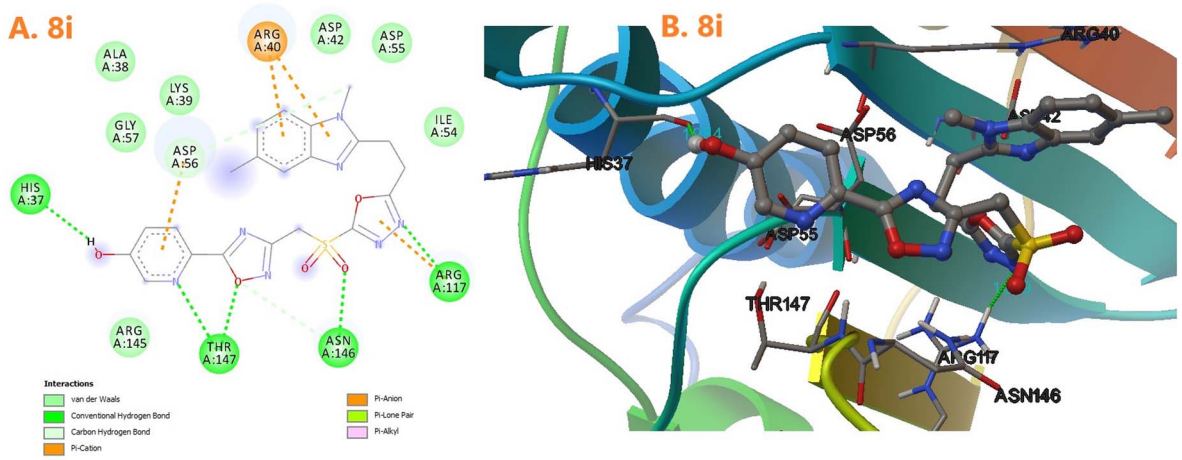


Fig. 5 Compound **8i** binds to the *E. Coli* topoisomerase IV active site (PDB code: 3FV5), as shown in (A) and (B), which display **8i**'s 3D and 2D interactions, respectively.

that the amine substituent pyridin-2-yl moiety (**8j**) was less active than the chloro substituent pyridin-2-yl on the 1,2,4-oxadiazole (**8k**).

The results of *in vitro* assessment of the antimicrobial efficacy of most active benzo[*d*]imidazoles **8b**, **8f**, **8i** and **8k** using MICs are tabulated in Table 2 and Fig. 1. MICs against *S. pyogenes* ATCC 19615, which indicate that the tested oxadiazoles are most effective at 7.3 ± 0.85 μM and that the lowest concentration considerably inhibits their development, followed by MXF at 8.2 ± 1.10 μM. On the other hand, the MICs of the investigated oxadiazole composites that had bactericidal effects on isolates of *S. aureus* ATCC 29213 and *S. epidermidis* ATCC 12228 were 9.2 ± 0.09 and 6.9 ± 1.01 μM for **8b** and **8i**, respectively. Similarly, MICs showed that the most effective analogues for *K. pneumoniae* ATCC 13883 were **8f** and **8i**, with 8.0 ± 1.03 and 19.3 ± 1.65 μM, respectively, followed by **8b**, with 27.4 ± 0.70 μM. The **8i** and **8k** oxadiazole composites were found to be the most effective at 7.0 ± 1.35 and 20.6 ± 1.60 μM, respectively, according to MICs against *E. coli* ATCC 25922. The **8b** compound came in second at 30.3 ± 1.20 μM. *S. aureus* ATCC 29213 was less susceptible to the antibacterial activity of compounds **8f** and **8k** (MIC = 40.2 ± 1.23, 37.1 ± 0.67 μM) with *m*-chloro and *o*-chloro on the phenyl ring of the 1,2,4-oxadiazole portion. When tested against *P. aeruginosa* ATCC 27853, compounds **8b** and **8i** (MIC > 50 μM) that had a nitro or hydroxy group on the phenyl ring of the 1,2,4-oxadiazole portion did not show antibacterial efficacy. The nitration and chlorination of the phenyl moiety at position 4th and 3rd with oxadiazole ring resulted in compounds that displayed good antimicrobial on both Gram-positive and Gram-negative strains. The lower activity of compounds bearing bulky groups *meta*-bromo and *meta*-nitro (*e.g.*, **8a** and **8e**) suggests steric hindrance or reduced interaction potential. This consistent correlation across *in vitro*, SAR, and docking data underscores the impact of electronic and

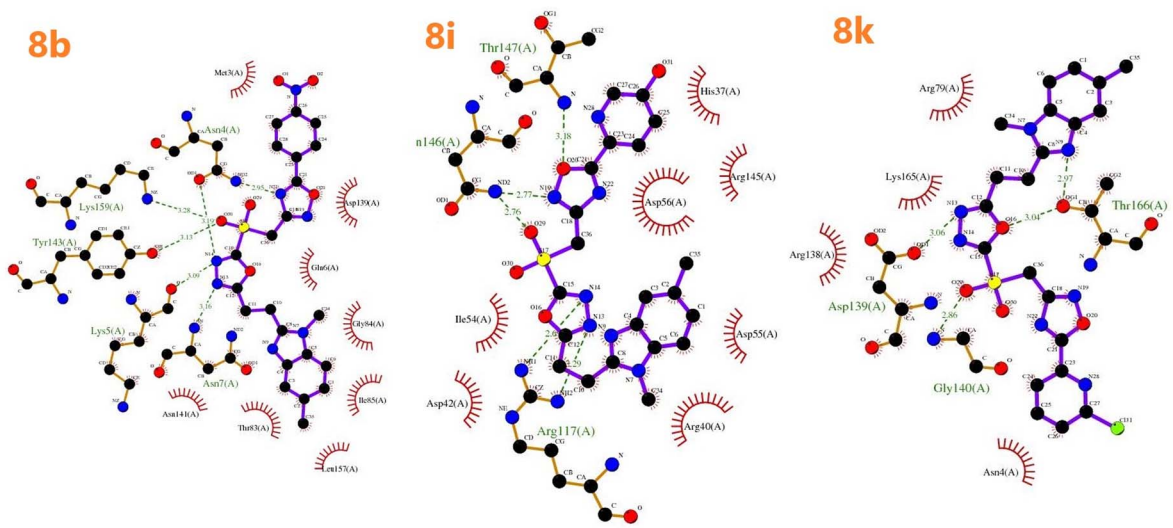


Fig. 6 The Ligplot interactions of **8b**, **8i**, and **8k** with the antibacterial protein active site are depicted in the figure, highlighting comparable important interactions inside the active site pockets.

Table 3 Different docking pose interactions in DNA GyrB and topoisomerase

| | Gram-positive strains | | |
|---|---|---|---|
| Entry | $\Delta G$ (kcal mol$^{-1}$)/(kl) | Interacting residues | Bond distance [Å] |
| **Antibacterial drug candidate *S. aureus* [4URN]** | | | |
| **8b** | −7.42/3.65 μM | Hydrogen bonding: AsnA:7, AsnA:4 × 2, AsnA:141, TyrA:143, LysA:159<br>π-donor hydrogen bonding: LysA:5 alkyl–alkyl: LeuA:157<br>π-anion: AspA:12, AspA:139<br>π-sulfur: ThrA:143<br>π-loan pair: ThrA:83<br>van der Waals: ProA:91, IleA:85, GlyA:84, GlnA:6 | >50 |
| **8k** | −8.10/32.22 μM | Hydrogen bonding: ThrA:166 × 2, GlyA:140, AspA:139 AsnA:146 × 2, ThrA:147, ArgA:117 × 2<br>Carbon H-bonding: ThrA:166<br>π-alkyl & alkyl–alkyl: ArgA:138, AlaA:2, ArgA:79<br>π-donor: H-bond: AspA:139<br>π-π stacking: AspA:139 × 2<br>van der Waals: AlaA:2, MetA:3, LysA:165, LysA:164, LysA:162, ThrA:163, AsnA:4 | 2.97, 3.04, 2.86, 3.06<br>3.22, 2.80 |
| **Antibacterial drug candidate *E. coli* [3FV5]** | | | |
| **8i** | −7.15/31.07 μM | Hydrogen bonding: HisA:37, ThrA:147 × 2, AsnA:146, ArgA:117 × 2<br>Carbon H-bonding: AspA:56, AsnA:146<br>π-cation: ArgA:40 × 2<br>π-anion: ArgA:117, AspA:56<br>van der Waals: AlaA:38, GlyA:57, LysA:39, AspA:42, AspA:55, IleA:54, ArgA:145 | 2.70, 3.18, 2.77, 2.76, 3.29,2.82<br>2.60, 2.89 |

steric features on biological efficacy. Additionally, heteroaryl substitutions, particularly pyridine-based analogues (**8i** and **8k**), showed improved antibacterial potency. This may be attributed to the presence of heteroatoms that facilitate additional hydrogen bonding and favorable interactions with bacterial enzymes, as supported by docking studies. The introduction of EWG ($NO_2$, Cl) substituents does contribute good activity than EDG ($CH_3$ and $NH_2$) groups. The ortho and meta positions of the phenyl group substituents were well tolerated, when compared to other substitution *via* para groups more beneficial and showed excellent antibacterial activity (Fig. 3).

It should be noted that the present biological evaluation is limited to planktonic antibacterial assays, which represents a limitation of the current study. Biofilm-associated and fungal infections are clinically more challenging and are not addressed here. However, previous reports have demonstrated that benzimidazole and oxadiazole scaffolds possess promising antifungal and antibiofilm activities, attributed to their ability to disrupt microbial membranes and interfere with biofilm formation pathways. Therefore, the benzo[*d*]imidazole-oxadiazole hybrids reported in this study may also hold potential for antifungal and antibiofilm applications, which will be explored in future investigations.

Table 4 Physicochemical and lead likeness properties of oxadiazole compounds (**8a–8k**)

| Entry | TPSA | *I* log *P* | *M* log *P* | log *S* (ESOL) | Lipinski | Ghose | Veber | Egan | Muegge | Leadlike ness | Bio. score | Brenk |
|---|---|---|---|---|---|---|---|---|---|---|---|---|
| **8a** | 184.0 | 2.38 | 1.50 | −4.70 | No | No | No | No | No | No | 0.17 | 2 |
| **8b** | 184.0 | 2.38 | 1.50 | −4.70 | No | No | No | No | No | No | 0.17 | 2 |
| **8c** | 158.4 | 2.56 | 1.79 | −4.51 | Yes | No | No | No | No | No | 0.55 | 0 |
| **8d** | 158.4 | 3.17 | 1.79 | −4.51 | Yes | No | No | No | No | No | 0.55 | 0 |
| **8e** | 138.1 | 3.33 | 2.87 | −5.55 | Yes | No | Yes | No | Yes | No | 0.55 | 0 |
| **8f** | 138.1 | 3.10 | 2.76 | −5.24 | Yes | No | Yes | No | Yes | No | 0.55 | 0 |
| **8g** | 138.1 | 3.77 | 2.50 | −4.95 | Yes | Yes | Yes | No | Yes | No | 0.55 | 0 |
| **8h** | 151.0 | 2.65 | 1.68 | −4.14 | Yes | No | No | No | No | No | 0.55 | 0 |
| **8i** | 171.3 | 2.76 | 0.81 | −3.86 | Yes | No | No | No | No | No | 0.55 | 0 |
| **8j** | 171.0 | 2.14 | 0.81 | −3.65 | Yes | No | No | No | No | No | 0.55 | 0 |
| **8k** | 151.0 | 2.79 | 1.79 | −4.80 | Yes | No | No | No | No | No | 0.55 | 1 |

### 2.2 Docking analysis

Molecular docking was done to make sure that strong ligands had an inhibitory mechanism. This research makes a substantial contribution to our knowledge of molecular biological profiles. We conducted a molecular docking study on the most active ligands that were found to be the most effective inhibitors in biological evaluation. We used the particular identifier codes 4URN for *S. aureus* GyrB and 3FV5 for *E. coli* Topoisomerase IV to retrieve the protein molecules from the RCSB Protein Data Bank (PDB).[39–42] Polar hydrogens were added after co-crystallized ligand and water molecules were removed from both proteins to prepare them for docking. Using the π-system of the enzyme, ligand molecules attach to the enzymes in the active site by π-cation, π-cation, π-donor H-bond, π-alkyl, π-loan pair, and π–π interactions, according to the results of the docking study.

In addition to these bonds, the potent compounds also displayed various forms of H-bonding, van der Waals, carbon H-bond, and alkyl–alkyl interactions (Fig. 4, 5, and 6). According to the dissociation constant of 3.65 μM and negative score energy values of −7.42 kcal $mol^{-1}$, respectively, compound **8b** formed the most stable complex with the *S. aureus* (PDB ID: 4URN) target. This molecule showed one electrostatic alkyl–alkyl interaction with LeuA:157 and one strong π-donor H-bond with LysA:5 (bond distance = 2.75 Å). Additionally, it demonstrated four hydrophobic van der Waals contacts with the *S. aureus* target's active site residue: ProA:91, IleA:85, GlyA:84, and GlnA:6 (Table 3 and Fig. 4). There are four strong conventional H-bonds that the compound's sulfonyl group established with TyrA:143 [O28···OD1], LysA:159 [O28···NZ], AsnA:4 [O21···OD1], and AsnA:141 [O21···NH] at bond distances of 3.13 Å, 3.28 Å, 2.86 Å, and 2.41 Å, respectively. Additionally, the π-sulfur bonding interaction seen with TyrA:143 can be related to the sulfonyl group. Since the sulfonyl gatekeeper residue frequently plays a critical role in inhibitor selectivity, these interactions are very intriguing. Extending from the core structure, the 1,3,4-oxadiazole group seems to establish two hydrogen connections with LysA:5 [N14···O, 3.09 Å] and AsnA:7 [N13···N, 3.16 Å], further solidifying the ligand's location [Fig. 6]. At the same time, 1,2,4-oxadiazole of this ligand formed one H-bond interaction *via* AsnA:4 residue [N22···NZ, 2.95 Å] and π-anion interaction *via* AspA:139 [3.18 Å] in the active site *S. aureus* target. A possibly high affinity and specificity for *S. aureus* is suggested by the compound's capacity to interact with numerous residues through its varied functional groups.

Notably, the compound **8k** complex with the *S. aureus* target (PDB code: 4URN) had a good dissociation constant of 32.22 μM and the best negative energy value of −8.10 kcal $mol^{-1}$. With the antibacterial target's active site, this molecule established three electrostatic π-alkyl and alkyl–alkyl ArgA:79, ArgA:138, and AlaA:2 contacts. Interestingly, these studies have shown that the amino acid AspA:139 × 2 [distance = 3.22 Å and 2.80 Å] plays a significant role in amide π-stacking in the inhibition of *S. aureus* receptors. GlyA:140 formed a hydrogen bond with the sulfonyl group's oxygen (O29, 2.86 Å) during the co-crystallized ligand's interaction. Two more π-donor hydrogen bonding contacts between AspA:139 and the 1,3,4-oxadiazole core and ThrA:167 and the sulfonyl moiety were discovered. The contact between the co-crystallized ligand entailed two bonds of hydrogen involving the region of the hinge (ThrA:166) with the

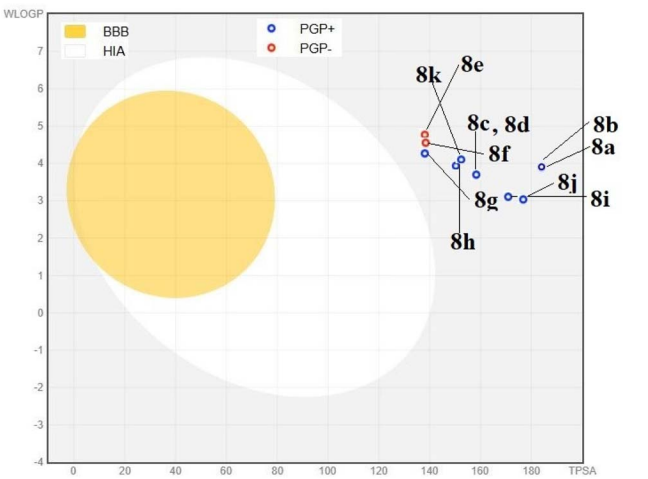


Fig. 8 The intestinal absorption and blood–brain barrier penetration of 1,3,4-oxadiazoles are represented by the boiled egg [**8a–8k**].

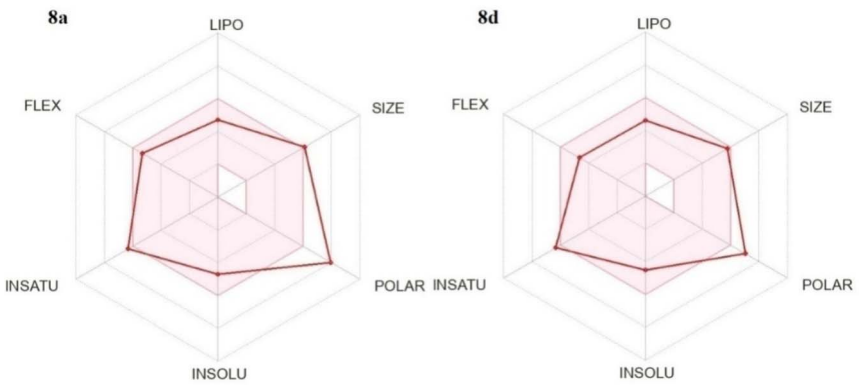


Fig. 7 Bioavailability radar of benzo[*d*]imidazole compounds **8a**, and **8d**.

1,3,4-oxadiazole and benzo[*d*]imidazole rings at a distance 3.04 and 2.97 Å accordingly (Fig. 4).

In addition, one extra hydrogen bonding interaction have been found between AspA:139 [3.06 Å] and the nitrogen of the 1,3,4-oxadiazole moiety (Fig. 6). In the binding pocket of *E. coli* Topoisomerase IV (PDB code: 3FV5), the *N*-methyl group of the benzo[*d*]imidazole ring of ligand8i connected with AspA:56 *via* a carbon H-bond. Furthermore, at a distance of 2.60 and 2.89 Å, the benzo[*d*]imidazole ring demonstrated π-cation interactions with the ArgA:40 × 2 residue. The antibacterial known inhibitor's 1,3,4-oxadiazole ring interacted with ArgA:117 *via* π-anion and H-bond interactions. Furthermore, hydroxy pyridine core of compound **8i** exhibited two strong hydrogen bonds (conventional types) with the residue HisA:37, and ThrA:147 respectively (bond distance = 2.96 Å and 2.75 Å) (Fig. 5). Seven electrostatic interactions (van der Waals) were detected with ArgA:145, GlyA:57, AlaA:38, LysA:39, AspA:42, AspA:55, and IleA:54, respectively. As a result, two typical H-bond contacts between the residues, ThrA:147 and AsnA:146, were formed between 1,2,4-oxadiazole and sulfonyl.

### 2.3 ADME-T analysis outcomes

The https://biosig.lab.uq.edu.au/pkcsm/prediction; and https://tox.charite.de/protox3/index.php?site=compound_input online servers were used to calculate ADME-T parameters.[43–45] *In silico* ADME-T (Absorption, Distribution, Metabolism, Excretion, and Toxicity) predictions are a crucial, cost-effective, and rapid method for screening compounds during the early stages of drug discovery. These computational tools allow for the assessment of drug-likeness and potential safety issues before synthesis, facilitating the selection of better lead candidates and reducing late-stage attrition. No more than one infraction of Lipinski's rule of five (ROF) is present in any of the synthesized benzo[*d*]imidazole-oxadiazole derivatives, which is acceptable. However, as evidenced by their low values for qualitative human oral absorption, these compounds are beyond the optimal range for expected aqueous solubility (ESOL). In spite of this, the synthesized oxadiazole shows significant *M* log *P* values [0.81 to 2.87] and low Caco-2 permeability values [−0.03 to −0.50], suggesting the possibility of intestinal absorption. The SwissADME

Table 5 Absorption, metabolism, excretion and toxicity results of benzo[*d*]imidazole compounds (**8a–8k**)

| Entry | 8a | 8b | 8c | 8d | 8e | 8f | 8g | 8h | 8i | 8j | 8k |
|---|---|---|---|---|---|---|---|---|---|---|---|
| **Absorption** | | | | | | | | | | | |
| Caco-2 | −0.49 | −0.50 | −0.27 | −0.30 | −0.32 | −0.32 | 0.33 | −0.03 | −0.08 | −0.05 | −0.16 |
| Skin per. | −2.73 | −2.73 | −2.73 | −2.73 | −2.73 | −2.73 | −2.73 | −2.73 | −2.73 | −2.73 | −2.73 |
| Pgp | Yes | Yes | Yes | Yes | Yes | Yes | Yes | Yes | Yes | Yes | Yes |
| VDss | −0.5 | −0.49 | −0.62 | −0.61 | −0.55 | −0.56 | −0.55 | −0.68 | −0.62 | −0.64 | −0.69 |
| BBB | −1.96 | −1.96 | −1.57 | −1.60 | −1.64 | −1.63 | −1.45 | −1.90 | −1.81 | −1.72 | −1.86 |
| CNS | −3.63 | −3.63 | −3.74 | −3.72 | −3.44 | −3.45 | −3.47 | −4.06 | −4.22 | −4.13 | −3.84 |
| **Metabolism** | | | | | | | | | | | |
| CYP1A2 | No | No | No | No | No | No | No | No | No | No | No |
| CYP2C19 | No | No | No | No | No | No | No | No | No | No | No |
| CYP2C9 | No | No | No | No | Yes | Yes | No | No | No | No | Yes |
| CYP2D6 | No | No | No | No | No | No | No | No | No | No | No |
| CYP3A4 | No | No | No | No | No | No | No | No | No | No | No |
| CYP2E1 | No | No | No | No | No | No | No | No | No | No | No |
| **Excretion** | | | | | | | | | | | |
| OCT 2 sub | Yes | Yes | No | No | Yes | Yes | Yes | Yes | No | No | No |
| T1/2 | −0.003 | 0.032 | 0.25 | 0.28 | 0.15 | 0.20 | 0.25 | 0.27 | 0.21 | 0.27 | 0.08 |
| **Toxicity** | | | | | | | | | | | |
| AMES | Yes | Yes | No | No | No | No | No | No | Yes | Yes | No |
| hERG I | No | No | No | No | No | No | No | No | No | No | No |
| hERG II | Yes | Yes | Yes | Yes | Yes | Yes | Yes | Yes | Yes | Yes | Yes |
| Skin. Sen | No | No | No | No | No | No | No | No | No | No | No |
| Hep. Tox. | Yes | Yes | Yes | Yes | Yes | Yes | Yes | Yes | Yes | Yes | Yes |
| Neuro Tox. | No | No | No | No | No | No | No | No | No | No | No |
| Cardi. Tox. | No | No | No | No | No | No | No | No | No | No | No |
| Carcino. city | Yes | Yes | Yes | No | Yes | Yes | Yes | No | Yes | Yes | Yes |
| Muta. city | Yes | Yes | No | No | No | No | No | No | No | No | No |
| Cytotox. | No | No | No | No | No | No | No | No | No | No | No |
| BBB-bar. | Yes | Yes | No | No | Yes | Yes | Yes | Yes | No | Yes | Yes |
| Eco. Tox. | Yes | Yes | No | No | Yes | Yes | No | No | No | No | No |
| Clinical Tox. | No | No | No | No | No | No | No | No | No | No | No |
| ER-alpha | No | No | No | No | No | No | No | No | No | No | No |
| GABA | No | No | No | No | No | No | No | No | No | No | No |
| Pregnane-X | No | No | No | No | No | No | No | Yes | No | No | No |

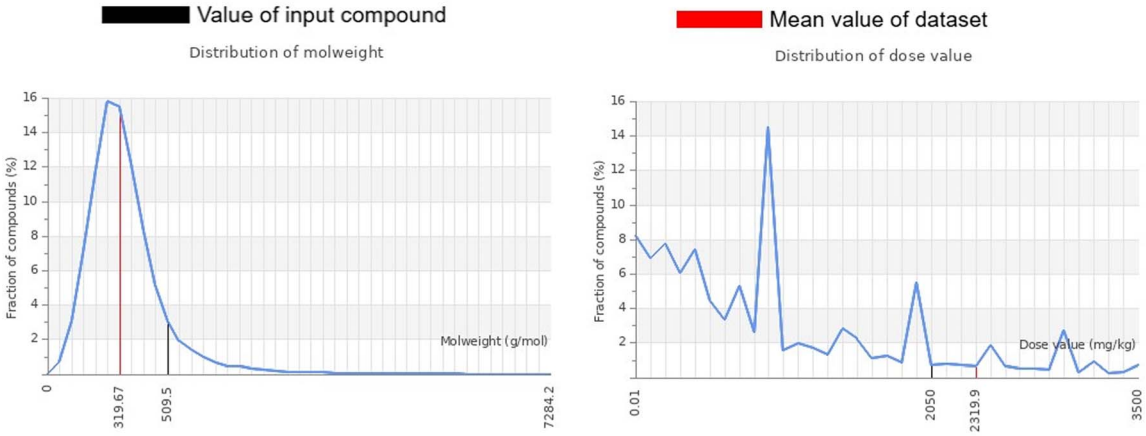


Fig. 9 Comparison of input compound (**8a**) with dataset compounds.

website calculates other metrics that fit within the recommended limitations, including the blood–brain partition coefficient, affinity to HIA, and topological polar surface area (TPSA), Ghose, Veber, Egan, Muegge, and Lead like ness (Table 4). Fig. 7 shows the bioavailability radar chart for the tested derivatives. Out of the six examined parameters—lipophilicity (LIPO), size, polarity, insolubility (INSOL), insaturation (INSATU), and flexibility (FLEX)—compounds **8a** and **8d** only exhibit one violation, and that was in the polarity parameter (Fig. 7). A BOILED-Egg, a two-dimensional figure that used estimated TPSA and A WLOGP features, was used to show the results. The most promising compound absorption across the blood–brain barrier (BBB) and human intestinal absorption (HIA) was shown in graphs. A BOILED-Egg chart was made, where the white region represented gastrointestinal absorption and the non-mutually exclusive yellow area represented BBB penetration. A blue hue indicates a high probability that the tested drug is a PGP substrate, whereas a red color indicates a lower probability. PGP is an efflux protein that is in charge of the uptake and efflux of several pharmaceuticals. All of the recently produced chemicals **8a–8k** are seen to lie inside the gray region of Fig. 8, suggesting that they are likely to be poorly absorbed *via* the GI tract by passive diffusion. Although they are outside the plot's range and may not be able to reach the brain, compounds **8a**, **8b**, **8i**, and **8j** have the ability to cross the blood–brain barrier. Furthermore, the Boiled-egg plot's red spots (**8e** and **8f**) indicate that the candidates are not *P*-glycoprotein (PGP) substrates, indicating good bioavailability as these compounds may be able to stop the reflux impact.

It also evaluates the bioavailability score and looks at cytochromes P450 molecular interactions (CYP). Since substances like 1A2, 2C19, 2C9, 2D6, 3A4, and $2 \times 10^1$ were expected to have minimal inhibitory activity on different CYP450 isozymes, drug–drug interactions are unlikely to happen. Crucially, no drug exhibited CYP2E1 inhibition, indicating a more specific metabolic profile. With the exception of compounds **8c**, **8d**, **8i**, **8j**, and **8k**, excretion predictions showed that none of the compounds were substrates for renal OCT2. The Ames test prediction evaluates the potential for genetic damage. A positive AMES alert *in silico* indicates a potential mutagenic risk. During optimization, such compounds are usually deprioritized, or the specific functional group responsible for the alert is identified and replaced to ensure the final candidate is non-mutagenic. All


Fig. 10 Toxicity model report of triazole **8a** and **8i**.

of the compounds' toxicity predictions were encouraging; none of them (except **8a**, **8b**, **8i**, and **8j**) displayed any indications of AMES toxicity, indicating a low probability of mutagenic consequences used to predict the toxicological endpoints and organ toxicities of ligands by the Protox-II service. The web server chose toxicity targets and computed the acute toxicity using selected models. The six different targets linked to pharmacological side effects served as the foundation for the anticipated amount of toxicity. The compounds' cytotoxicity, carcinogenicity, neurotoxicity, cardiotoxicity, hepatotoxicity, and mutagenicity were evaluated (Table 5). *In silico*, hepatotoxicity is often predicted based on structural alerts or machine learning models (*e.g.*, HepG2 cytotoxicity). If a lead compound shows high hepatotoxicity potential, it suggests that structural modifications (*e.g.*, reducing lipophilicity or modifying metabolically active sites) may be required to decrease liver toxicity. All the oxadiazole compounds showed hepatotoxicity, while compounds **8d** and **8h** were showed to be non-carcinogenic. Furthermore, compounds **8a** and **8b** shown mutagenicity, while compounds **8a**, **8b**, **8e**, and **8f**, respectively, demonstrated ecotoxicity (Table 4). The active cluster of physicochemical regions for optimal oral bioavailability (hepatotoxicity, neurotoxicity, cardiotoxicity, *etc.*) is shown by the blue color radar, whereas the inactive cluster is represented by the orange color radar (Fig. 9 and 10). All things considered, these ADME-T predictions demonstrate the advantageous pharmacokinetic advantageous and safety characteristics of compounds **8a–8k**, which make them attractive options for additional therapeutic agent development.

# 3 Conclusion

A set of innovative benzo[*d*]imidazole-oxadiazole derivatives (**8a–8k**) was developed and produced using six step component procedures. Compound structures were verified *via* HRMS characterizations, $^{1}$H-NMR, $^{13}$C-NMR, and FT-IR. The antibacterial efficiency of the studied molecules was assessed, and the majority of the compounds under investigation showed encouraging antimicrobial qualities. According to an *in vitro* assessment of antibacterial activity, molecule **8f** showed encouraging potency as an inhibitor of *K. pneumonia* and *P. aeruginosa*, with an MIC value of 8.0 ± 1.03, 10.5 ± 1.22 μM compared to GMF (MIC = 10.5 ± 1.01 & 11.3 ± 0.54 μM). Furthermore, it was observed that molecule **8b**, **8f** and **8i** exhibited an excellent inhibitory antibacterial effect on *E. coli* ATCC 25922, as indicated by its ZI values of 34 ± 1.12, 28 ± 0.10, and 36 ± 0.13 mm accordingly. The compound **8k** produced more potent antibacterial activity on *S. pyogenes*, and *S. aureus* (ZI = 26 ± 0.32 & 32 ± 0.80 mm), respectively, in comparison to MXF and GMF. Compounds having electron-withdrawing groups, on the other hand, exhibit more antibacterial action. By illustrating interactions such π-cation, π-sigma, H-bonds, CH-bonding, halogen bonds, van der Waals, π-alkyl, and the π-anion cloud, the results corroborate the experimental findings. Moreover, molecules **8b**, **8k**, and **8i** demonstrated the highest docking scores of −7.42, −8.10, and −7.15 kcal mol$^{-1}$ in *in silico* tests conducted on the most potent compounds with *S. aureus* (4URN) and *E. coli* (3FV5) enzymes. Likewise, *in silico* ADME/Tox discovered the drug-like properties of the proposed molecule, demonstrating its novelty as a potential lead. None of the compounds violated the Lipinski and Veber standards, and all of them, with the exception of **8a** and **8b**, fell within the expected range. Collectively, these findings underscore the potential of bis-oxadiazole hybrids, particularly compounds **8b** and **8f**, as promising leads for the development of new antimicrobial agents.

# Author contributions

Yellamanda Rao Salluri contributed the synthetic work and data analysis. Kalyani Chepuri has contributed the biological evaluation. SA has contributed ideology and concept.

# Conflicts of interest

There are no conflicts to declare.

# Data availability

The data supporting this article have been included as part of the supplementary information (SI). Supplementary information is available. See DOI: https://doi.org/10.1039/d5ra09260d.

# Acknowledgements

The authors YRS and SA thankful to VFSTR for providing the infrastructure to conduct the research work. SA greatly acknowledges ANRF (*i.e.*, formerly DST-SERB) for providing financial support under TARE (TAR/2022/000207). The author YRS is thankful to Curia for providing NOC as well as extensive support.

# References

1 N. R. Kumar, T. A. Balraj, S. N. Kempegowda and A. Prashant, *Antibiotics.*, 2024, **13**, 46.
2 W. Xue, X. Zuo, X. Zhao, X. Wang, X. Zhang, J. Xia, M. Cheng and H. Yang, *Bioorg. Chem.*, 2024, **147**, 107314.
3 M. Chalkha, M. Akhazzane, F. Z. Moussaid, O. Daoui, A. Nakkabi, M. Bakhouch, S. Chtita, S. Elkhattabi, A. I. Housseini and M. El. Yazidi, *New J. Chem.*, 2022, **46**, 2747.
4 R. Lucas, Y. Hadizamani, J. Gonzales, B. Gorshkov, T. Bodmer, Y. Berthiaume, U. Moehrlen, H. Lode, H. Huwer, M. Hudel, M. A. Mraheil, H. A. F. Toque, T. Chakraborty and J. Hamacher, *Toxins*, 2020, **12**, 223.
5 S. Kumar, S. Gupta, V. Rani and P. Sharma, *Med. Chem.*, 2022, **18**, 831.
6 J. S. Lim, Y. Y. Chai, W. X. Ser, A. V. Haeren, Y. H. Lim, T. Raja, J. B. Foo, S. Hamzah, R. Sellappans and H. Y. Yow, *Iran. J. Basic Med. Sci.*, 2024, **27**, 134.
7 (*a*) C. E. Theodore, S. B. B. Prasad, K. Y. Kumar, M. S. Raghu, F. Alharethy, M. K. Prashanth and B.-H. Jeon, *J. Mol. Struct.*, 2024, **1302**, 137521; (*b*) T. Jain, P. R. Muktapuram,

K. Sharma, O. Ravi, G. Pant, K. Mitra, S. R. Bathula and D. Banerjee, *Bioorg. Med. Chem. Lett.*, 2018, **28**, 1776; (*c*) T. Jain, P. R. Muktapuram, S. Pochampalli, K. Sharma, G. Pant, K. Mitra, S. R. Bathula and D. Banerjee, *J. Med. Microbiol.*, 2017, **66**, 1706.

8 A. Baron, C. L. Sann and J. Mann, *Bioorg. Med. Chem.*, 2022, **58**, 116656.

9 R. S. Kankate, P. S. Gide and D. P. Belsare, *Arabian J. Chem.*, 2019, **12**, 2224.

10 M. Ashfaq, S. S. Shah, T. Najam, M. M. Ahmad, R. Tabassum and G. Rivera, *Curr. Med. Chem.*, 2014, **21**, 911.

11 N. Su, Q. Wang, H. Y. Liu, L. M. Li, T. Tian, J. Y. Yin, W. Zheng, Q. X. Ma, T. T. Wang, T. Li, T. L. Yang, J. M. Li, N. C. Diao, K. Shi and R. Du, *Front. Vet. Sci.*, 2023, **9**, 1086180.

12 Y. Bansal and O. Silakari, *Bioorg. Med. Chem.*, 2012, **20**, 6208.

13 K. P. Barot, S. Nikolova, I. Ivanov and M. D. Ghate, *Mini-Rev. Med. Chem.*, 2013, **13**, 1421.

14 R. S. Keri, A. Hiremathad, S. Budagumpi and B. M. Nagaraja, *Chem. Biol. Drug Des.*, 2015, **86**, 19.

15 W. Akhtar, M. F. Khan, G. Verma, M. Shaquiquzzaman, M. A. Rizvi and S. H. Mehdi, *Eur. J. Med. Chem.*, 2017, **126**, 705.

16 B. Dik, D. Coskun, E. Bahcivan and K. Uney, *Turk. J. Med. Sci.*, 2021, **51**, 1579.

17 A. B. Popov, L. Krstulovic, S. Kostrun, D. Jelic, A. Bokulic, M. R. Stojkovic, I. Zonjic, M. C. Taylor, J. M. Kelly and M. Bajic, *Eur. J. Med. Chem.*, 2020, **207**, 112802.

18 B. Bhrigu, N. Siddiqui, D. Pathak, M. S. Alam, R. Ali and B. Azad, *Acta Pol. Pharm.*, 2012, **69**, 53.

19 S. V. Bhandari, O. G. Nagras, P. V. Kuthe, A. P. Sarkate, K. S. Waghamare, D. N. Pansare, S. Y. Chaudhari, S. N. Mawale and M. C. Belwate, *J. Mol. Struct.*, 2023, **1276**, 134747.

20 S. Z. B. Bohurudeen, A. Ambala, T. R. Allaka, M. Z. Ahmed, B. Thirunavukkarasu, R. Tirumalareddy and S. Venkatesan, *J. Mol. Struct.*, 2025, **1322**, 140251.

21 Z. Wu, M.-B. Xia, D. Bertsetseg, Y.-H. Wang, X.-L. Bao, W.-B. Zhu, X. Tao, P.-R. Chen, H.-S. Tang, Y.-J. Yan and Z.-L. Chen, *Bioorg. Chem.*, 2020, **101**, 104042.

22 R. K. Salahuddin and J. K. Sahu, *Curr. Drug Res. Rev.*, 2021, **13**, 90.

23 G. R. Venkateswara, T. R. Allaka, M. K. Gandla, V. N. P. K. Veera, S. R. Pindi, P. R. R. Vaddi and H. B. Bollikolla, *J. Heterocycl. Chem.*, 2023, **60**, 1666.

24 S. Wang, H. Liu, X. Wang, K. Lei, G. Li, J. Li, R. Liu and Z. Quan, *Eur. J. Med. Chem.*, 2020, **206**, 112672.

25 T. Glomb, K. Szymankiewicz and P. Swiatek, *Molecules*, 2018, **23**, 3361.

26 F. Peng, T. Liu, Q. Wang, F. Liu, X. Cao, J. Yang, L. Liu, C. Xie and W. Xue, *J. Agric. Food Chem.*, 2021, **69**, 11085.

27 G. Chawla, B. Naaz and A. A. Siddiqui, *Mini-Rev. Med. Chem.*, 2018, **18**, 216.

28 B. A. Khan, S. S. Hamdani, S. Jalil, S. A. Ejaz, J. Iqbal, A. M. Shawky, A. M. Alqahtani, G. A. Gabr, M. A. A. Ibrahim and P. A. Sidhom, *Pharmaceuticals*, 2023, **16**, 11.

29 T. M. Dhameliya, S. J. Chudasma, T. M. Patel and B. P. Dave, *Mol. Diversity*, 2022, **26**, 2967.

30 P. H. Parikh, J. B. Timaniya, M. J. Patel and K. P. Patel, *Med. Chem. Res.*, 2020, **29**, 538.

31 M. Zhou, J. C. Boulos, E. A. Omer, S. M. Klauck and T. Efferth, *Molecules*, 2023, **28**, 5658.

32 U. A. Atmaram, P. K. Gadekar, H. Sivaramakrishnan, N. Naik, V. M. Khedkar, D. Sarkar, A. Choudhari and S. R. Mohana, *Bioorg. Chem.*, 2019, **86**, 507.

33 D. K. Meher, A. K. Nayak, A. K. Singh and M. Pathak, *J. Pharmacogn. Phytochem.*, 2020, **9**, 1307.

34 F. S. Fernandes, H. Santos, S. R. Lima, C. Conti, M. T. Rodrigues, L. A. Zeoly, L. L. G. Ferreira, R. Krogh, A. D. Andricopulo and F. Coelho, *Eur. J. Med. Chem.*, 2020, **201**, 112418.

35 S. Gandamalla, S. Mavurapu, K. Sambaru and T. R. Allaka, *J. Chin. Chem. Soc.*, 2025, **72**, 721.

36 A. Tejeswara Rao, K. Bhaskar, P. Naveen, K. Naveen, C. Kalyani and A. Jaya Shree, *Mol. Diversity*, 2022, **26**, 1581.

37 S. C. Karad, V. B. Purohit, R. P. Thummar, B. K. Vaghasiya, R. D. Kamani, P. Thakor, V. R. Thakkar, S. S. Thakkar, A. Ray and D. K. Raval, *Eur. J. Med. Chem.*, 2017, **126**, 894.

38 S. Mirzayi, M. Kakanj, S. Sepehri, B. Alavinejad, Z. Bakherad and M. Ghazi-Khansari, *Phosphorus, Sulfur Silicon Relat. Elem.*, 2021, **196**, 1109.

39 G. M. Morris, R. Huey, W. Lindstrom, M. F. Sanner, R. K. Belew, D. S. Goodsell and A. J. Olson, *J. Comput. Chem.*, 2009, **16**, 2785.

40 J. Lu, S. Patel, N. Sharma, S. M. Soisson, R. Kishii, M. Takei, Y. Fukuda, K. J. Lumb and S. B. Singh, *ACS Chem. Biol.*, 2014, **9**, 2023.

41 R. A. Laskowski, J. Jabłońska, L. Pravda, R. S. Vařeková, J. M. J. B. Baell and G. A. Holloway, *J. Med. Chem.*, 2010, **53**, 2719.

42 N. M. O'Boyle, M. Banck, C. A. James, C. Morley, T. Vandermeersch and G. R. Hutchison, *J. Cheminf.*, 2011, **3**, 33.

43 A. B. Reddy, T. R. Allaka, V. S. R. Avuthu, P. V. V. N. Kishore and H. Nagarajaiah, *ChemistrySelect*, 2024, **9**, e202401989.

44 A. Daina, O. Michielin and V. J. S. Zoete, *Sci. Rep.*, 2017, **7**, 42717.

45 P. Banerjee, A. O. Eckert, A. K. Schrey and R. Preissner, *Nucleic Acids Res.*, 2018, **46**, W257.